Atmos. Chem. Phys. Discuss., 15, 32367–32412, 2015
www.atmos-chem-phys-discuss.net/15/32367/2015/
doi:10.5194/acpd-15-32367-2015

Atmospheric Chemistry and Physics Discussions

Modeling of the anthropogenic heat flux and its effect on air quality over the Yangtze River Delta region, China

M. Xie, J. Liao, T. Wang, K. Zhu, B. Zhuang, Y. Han, M. Li, and S. Li

School of Atmospheric Sciences, Nanjing University, Nanjing, 210093, China

Received: 6 October 2015 – Accepted: 31 October 2015 – Published: 18 November 2015

Correspondence to: M. Xie (minxie@nju.edu.cn) and T. Wang (tjwang@nju.edu.cn)

Published by Copernicus Publications on behalf of the European Geosciences Union.

Abstract

Anthropogenic heat (AH) emissions from human activities caused by urbanization can affect the city environment. Based on the energy consumption and the gridded demographic data, the spatial distribution of AH emission over the Yangtze River Delta (YRD) region is estimated. Meanwhile, a new method for the AH parameterization is developed in the WRF/Chem model, which incorporates the gridded AH emission data with the seasonal and the diurnal variations into the simulations. By running this upgraded WRF/Chem for two typical months in 2010, the impacts of AH on the meteorology and air quality over the YRD region are studied. The results show that the AH fluxes over YRD have been growing in recent decades. In 2010, the annual mean values of AH over Shanghai, Jiangsu and Zhejiang are 14.46, 2.61 and 1.63 $W m^{-2}$ respectively, with the high values of 113.5 $W m^{-2}$ occurring in the urban areas of Shanghai. These AH emissions can significantly change the urban heat island and urban-breeze circulations in the cities of the YRD region. In Shanghai, 2 m air temperature increases by 1.6 °C in January and 1.4 °C in July, the planetary boundary layer height rises up by 140 m in January and 160 m in July, and 10 m wind speed is enhanced by 0.7 $m s^{-1}$ in January and 0.5 $m s^{-1}$ in July, with higher increment at night. And the enhanced vertical movement can transport more moisture to higher levels, which causes the decrease of water vapor at the ground level and the increase in the upper PBL, and thereby induces the accumulative precipitation to increase by 15–30 % over the megacities in July. The adding AH can impact the spatial and vertical distributions of the simulated pollutants as well. The concentrations of primary air pollutants decrease near surface and increase at the upper levels, due mainly to the increases of PBLH, surface wind speed and upward air vertical movement. But surface O_3 concentrations increase in the urban areas, with maximum changes of 2.5 ppb in January and 4 ppb in July. Chemical direct (the rising up of air temperature directly accelerate surface O_3 formation) and indirect (the decrease in NO_x at the ground results in the increase of surface O_3) effects can play a significant role in O_3 changes over this region. The meteorology and air pollution

ACPD
15, 32367–32412, 2015

predictions in and around large urban areas are highly sensitive to the anthropogenic heat inputs, suggesting that AH should be considered in any climate and air quality assessment.

1 Introduction

Nearly all energy used for human purposes can eventually turn into anthropogenic heat (AH) within Earth's land–atmosphere system (Flanner, 2009; Chen et al., 2012). According to the distinctive human activities all over the world, this heat flux might vary spatially and temporally. On the global scale, the averaged value of AH flux has been estimated to be only 0.028 $W m^{-2}$. But it can reach to 0.39, 0.68 and 0.22 $W m^{-2}$ respectively over the continental United States, Western Europe and China (Flanner, 2009). In the densely populated and economically vibrant urban areas, the AH fluxes have been reported to typically range from 20 to 70 $W m^{-2}$ (Crutzen, 2004; Sailor and Lu, 2004; Fan and Sailor, 2005; Pigeon et al., 2007; Lee et al., 2009), whereas the fluxes might occasionally exceed the value of 100 $W m^{-2}$ as well (Quah and Roth, 2012; Xie et al., 2015). Under some extreme conditions, the magnitude of AH fluxes in cities can be a substantial heat source equivalent to the daily mean solar forcing (Ichinose et al., 1999; Hamilton et al., 2009; Iamarino et al., 2012), with a high value of 1590 $W m^{-2}$ reported in the densest part of Tokyo at the peak of air-conditioning demand (Ichinose et al., 1999). Consequently, accurate prediction of AH emissions is always a key issue that can improve our understanding of human impacts on urban climate and environment.

Anthropogenic heat can increase turbulent fluxes in sensible and latent heat, which might result in the atmosphere reserving more energy (Oke, 1988). Thus, the above-mentioned heat fluxes exhausted from human activities in cities can exert a significant influence on the dynamics and thermodynamics of urban boundary layer (Ichinose et al., 1999; Block et al., 2004; Fan and Sailor, 2005; Chen et al., 2009, 2012; Bohnenstengel et al., 2014), and thereby change the surface meteorological conditions (Khan

ACPD
15, 32367–32412, 2015

and Simpson, 2001; Block et al., 2004; Fan and Sailor, 2005; Ferguson and Woodbury, 2007; Chen et al., 2009; Zhu et al., 2010; Menberg et al., 2013; Wu and Yang, 2013; Feng et al., 2014; Bohnenstengel et al., 2014). Most previous studies of AH have focused on these effects. For instance, some researchers have found that AH strengthens the vertical movement of urban surface air flow, change the urban heat island circulation, and make the urban boundary layer more turbulent and unstable (Ichinose et al., 1999; Block et al., 2004; Fan and Sailor, 2005; Chen et al., 2009; Bohnenstengel et al., 2014). Others showed that AH in cities can result in significant and extensive warming, and tend to cause urban air temperatures to increase by several degrees (Fan and Sailor, 2005; Ferguson and Woodbury, 2007; Chen et al., 2009; Zhu et al., 2010; Menberg et al., 2013; Wu and Yang, 2013; Feng et al., 2014; Bohnenstengel et al., 2014). Moreover, Feng et al. (2014) reported that AH enhances the convergence of water vapor and rainfall amounts over urbanized areas, and changes the regional precipitation patterns to some extent. Urban air quality and local meteorological condition are inextricably linked. Therefore, all the findings above are likely to have important implications for air quality in urban areas as well. However, in the past, few researchers paid attention to this issue, and only a couple of studies have estimated the effects of AH on air pollutants (Ryu et al., 2013; Yu et al., 2014; Yang et al., 2014).

Over the past decades, along with the accelerated urbanization process and rapid economic development, many cities in China have been suffering the successive deterioration of air quality (Xie et al., 2014). Located in the coastal region in East China, the Yangtze River Delta (YRD) region also experienced a rapid urban expansion with the urbanization rate as high as 70 % and suffered from air pollutions (Liao et al., 2015). Consequently, several previous studies have tried to figure out the effects of urbanization on the severe atmospheric environmental problems in this region. For example, by using WRF/Chem model, Wang et al. (2009) quantified that the urban sprawl in YRD region has caused surface O_3 to increase by 2.9–4.2 % during the daytime and 4.7–8.5 % at night. And employing the WRF/CMAQ model, Li et al. (2011) showed that ozone (O_3) and haze problem had become an important issue due to the increasing of

ACPD
15, 32367–32412, 2015

urban land-use over the YRD region. Liao et al. (2015) further quantified the increase of O_3 and the decrease of PM_{10} or NO_x that can be attributed to the urban expansion. However, the above studies only took the expansion of urban land-use into account. We still need to know how the excessive anthropogenic heat from urban expansion impacts on urban climate and air quality. Among previous studies, a couple of researchers have tried to fill the knowledge gap. For instance, He et al. (2007) incorporated AH into a PBL (planetary boundary layer) model for Nanjing 2002 and found a temperature increase (0.5–1 °C) at night. Wang et al. (2015) reported that AH can cause notable warming in almost the whole YRD, which is more significant in winter than in summer. Unfortunately, these studies only focused on the effects of AH on local meteorological fields. Till now, none studies have evaluated the influence of AH on air quality over the YRD region.

The main purpose of this study is to improve our understanding about the influence mechanism of anthropogenic heat on atmospheric environment, especially in the typical polluted areas of China such as the YRD region. Consequently, in this paper, we focus on (1) quantifying the spatial and temporal distribution of AH emissions in the YRD region, (2) implementing of the gridded AH data into the modified WRF/Chem model with improved AH flux parameterization, and (3) evaluating the impacts of AH fluxes on meteorological condition and air quality over the YRD region. Detailed descriptions about the estimating method for anthropogenic heat flux over the YRD region, the adopted air quality model with configuration, and the observation data for model evolution are given in Sect. 2. Main results, including the spatial and temporal distribution of AH, the performance of WRF/Chem, and the exact impacts of AH on urban climate and air quality are presented in Sect. 3. In the end, a summary is given in Sect. 4.

ACPD
15, 32367–32412, 2015

2 Methodology

2.1 Anthropogenic heat flux modeling

We estimate the AH fluxes during the period from 1990 to 2010 over the area between (117° E, 28° N) and (123° E, 34° N), which covers the YRD region including Shanghai, southern Jiangsu province and northern Zhejiang province (shown in Fig. 1). In order to get the spatial distribution, this study area is also gridded as 144 rows and 144 columns with the grid spacing of 2.5 arcmin (approximately 4 km).

The anthropogenic heat flux Q_F ($W m^{-2}$) is the rate at which waste energy is discharged by human activities to the surroundings (Iamarino et al., 2012). In urban areas, it usually consists of the heat flux deriving from energy consumption in buildings ($Q_{F,B}$), from the transportation sector ($Q_{F,T}$) and from human metabolism ($Q_{F,M}$) (Grimmond, 1992; Sailor and Lu, 2004; Allen et al., 2010; Iamarino et al., 2012; Quah and Roth, 2012). Three general approaches have been recognized to estimate these terms (Sailor, 2011), including the building energy modeling approach for the building sector (Kikegawa et al., 2003), the closure of the energy budget (Offerle et al., 2005), and the use of statistics on energy consumption (Sailor and Lu, 2004; Flanner, 2009; Hamilton et al., 2009; Lee et al., 2009; Allen et al., 2010; Iamarino et al., 2012; Quah and Roth, 2012). The third method, which is also called the top-down energy inventory method, was the most common approach and widely applied in AH flux predictions in China (Chen et al., 2012; Lu et al., 2014; Xie et al., 2015). Based on these previous investigations, Q_F in this study is calculated by the following equation:

$$Q_F = Q_{F,I} + Q_{F,B} + Q_{F,T} + Q_{F,M} \quad (1)$$

where $Q_{F,I}$ represents the heat emitted from the industry sector ($W m^{-2}$).

According to the second law of thermodynamics, most energy used for human economy is immediately dissipated as heat, other energy temporarily stored as electrical, mechanical, chemical or gravitational potential energy can finally transform to high entropy thermal energy as well, and only a neglectful portion ($\ll 1\,\%$) might convert to

ACPD
15, 32367–32412, 2015

radiation and escape to space (Flanner, 2009). So, it is reasonable to assume that all non-renewable primary energy consumption is dissipated thermally in Earth's atmosphere. From another perspective, in this study, the gridded AH data is finally incorporated into the single layer urban canopy model SLUCM (Kusaka and Kimura, 2004; Chen et al., 2011), in which we do not need to strictly distinguish different sources of AH. In a consequent, $Q_{F,I} + Q_{F,B} + Q_{F,T}$ at each grid can be estimated on the basis of energy consumption from non-renewable sources (coal, petroleum, natural gas, and electricity etc.) by using the following equation:

$$Q_{F,I} + Q_{F,B} + Q_{F,T} = \eta \cdot \varepsilon_s \cdot C_s / (t \cdot A) \quad (2)$$

where, C_s is the primary energy consumption that has been converted to standard coal (t) at a grid. ε_s is the calorific value of standard coal (the conversion factor from primary energy consumption to heat), which is recommended to be 29 271 kJ kg^{-1} in many previous studies (Chen et al., 2012; Lu et al., 2014; Xie et al., 2015). η is the efficiency of heat release in different sectors, with the typical value of 60 % for electricity or heat-supply sector and 100 % for other sectors (Lu et al., 2014). t is the time duration of used statistic data, and is set to be 365 (days in a year) $\cdot$ 24 $\cdot$ 3600 = 31 536 000 s in this study. A represents the area of a grid, which is about 4 km $\times$ 4 km. To quantify the values of C_s, the authoritative statistics of annual standard coal consumption from 1990 to 2010 in provincial level are firstly obtained from China Statistical Yearbooks and the Yearbooks in Shanghai, Jiangsu and Zhejiang. Then, the total provincial energy consumption is apportioned to each grid according to population density and converted to annual-mean gridded energy flux. The population density with the resolution of 2.5 $\times$ 2.5 arcmin in 1990, 1995, 2000, 2005 and 2010 can be downloaded from Columbia University's Socioeconomic Data and Applications Center (http://sedac.ciesin.columbia.edu/gpw). That for 2010 is shown in Fig. 1b for example.

With respect to the heat flux generated by the human metabolism ($Q_{F,M}$), the grid value is computed as:

$$Q_{F,M} = P_g \cdot (M_d \cdot 16 + M_n \cdot 8)/24 \quad (3)$$

ACPD
15, 32367–32412, 2015

where P_g is the population at a grid. M_d and M_n represent the average human metabolic rate (W person^{-1}) during the daytime and nighttime. 16, 8 and 24 are the hours of daytime, nighttime and a whole day, respectively. Following the previous research work (Sailor and Lu, 2004; Chen et al., 2012; Lu et al., 2014; Xie et al., 2015), we assume that the sleeping metabolic rate M_d for a typical man is 75 W, and the average daytime metabolic rate M_n in urban areas is 175 W.

2.2 Air quality model and configuration

The WRF/Chem version 3.5 is applied to investigate the impacts of AH fluxes on climate and air quality over the YRD region. WRF/Chem is a new generation of air quality modeling system developed at National Center for Atmospheric Research (NCAR), in which the meteorological component (WRF) and the air quality component (Chem) are fully coupled using the same coordinates and physical parameterizations. The feedbacks between meteorology and air pollutants are included in the model. It has been proved to be a reliable tool in simulating air quality from city-scale to meso-scale in China (Liu et al., 2013; Yu et al., 2014; Liao et al., 2014, 2015).

As shown in Fig. 2a, three nested domains are used in this study, with the grid spacing of 81, 27 and 9 km, respectively. The outermost domain (Domain 1, D01) covers most of the East Asia and South Asia, the second domain (Domain 2, D02) covers central-east part of China, and the finest domain (Domain 3, D03) centered at Nanjing covers the entire YRD region (Fig. 2b). For all domains, from the ground level to the top pressure of 50 hPa, there are 36 vertical sigma layers with about 10 in the PBL. And the height of the lowest level is about 25 m.

Two simulation cases are conducted. One incorporates the urban canopy model with the gridded AH fluxes that are estimated in Sect. 2.1 (referred to as ADDAH case hereafter). The other only applies the same model but ignores the contribution of AH (referred to as NONAH case hereafter). To exclude the uncertainty conceivably caused by different configurations, all the physical schemes, chemical schemes and emission

ACPD
15, 32367–32412, 2015

inventory are the same in both NONAH and ADDAH simulations. Thus, the difference between the modeling results of NONAH and ADDAH can demonstrate the impacts of anthropogenic heat. In the YRD region, January and July can be representative of dry and wet season, respectively (Liao et al., 2015). Consequently, two time periods are chosen for simulations and analysis. One is from 00:00 UTC, 1 January to 00:00 UTC, 1 February 2010, and the other is from 00:00 UTC, 1 July to 00:00 UTC, 1 August 2010, which also match the time when observation data are available.

The detailed options for the physical and chemical parameterization schemes used in this study are shown in Table 1. The major selected physical options include Purdue Lin microphysics scheme, RRTM (Rapid Radiative Transfer Model) long-wave radiation scheme, Goddard short-wave radiation scheme, Kain–Fritsch cumulus parameterization scheme, Noah/LSM (Land Surface Model) scheme and MYJ (Mellor–Yamada–Janjic) PBL scheme. Specially, SLUCM (coupled with Noah/LSM) is adopted for better simulating the urban effect on meteorological conditions and pollutant distribution. The 30 s MODIS 20 category land datasets (Fig. 2b) are used to replace the default USGS (U.S. Geological Survey) land-use data, because USGS data are too outdated to illustrate the intensive land cover change over the YRD region. And the default values for urban canopy parameters in SLUCM, such as building morphometry, urban fraction and roughness length etc., are replaced by the typical values in the YRD region as well, following the work of He et al. (2007) and Liao et al. (2015). The initial meteorological fields and boundary conditions (forced every 6 h) are from NCEP global reanalysis data with $1^{\circ} \times 1^{\circ}$ resolution.

With respect to the major chemical options, the CBM-Z gas-phase chemistry scheme and the MOSAIC aerosol scheme are chosen. CBM-Z (Carbon-Bond Mechanism version Z) contains 55 prognostic species and 134 reactions (Zaveri and Peters, 1999). In MOSAIC (Model for Simulating Aerosol Interactions and Chemistry), the aerosol size distribution is divided into eight discrete size bins (Zaveri et al., 2008). Besides, aerosol direct and indirect effects through interaction with atmospheric radiation, photolysis, and microphysics routines are also taken into account in our simulations. The model-

ACPD
15, 32367–32412, 2015

ing results from the global chemistry transport model MOZART-4 are used to provide the initial chemical state and boundary conditions as described by Liao et al. (2015). The anthropogenic emissions are mainly from the inventory developed for the NASA INTEX-B mission (Zhang et al., 2009), and modified for simulations in the YRD region (Liao et al., 2014; 2105). The ammonia emission and biomass burning emissions, which are not contained in the INTEX-B inventory, are obtained from the inventory developed for TRACE-P (Streets et al., 2003). For Shanghai area, we use the additional 1 km × 1 km source emission compiled by Shanghai Environmental Monitoring Center during EXPO 2010 (Wang et al., 2012). And the biogenic emissions are estimated by using MEGAN2.04 (Guenther et al., 2006).

2.3 Methodology for incorporating gridded AH emission data

Within the Single Layer Urban Canopy Model SLUCM, the AH for each grid is determined by the fixed AH value for the urban land-use category, the fixed temporal diurnal pattern and the urban fraction value on each grid (Chen et al., 2011). AH with its diurnal variation is generally considered by adding them to the sensible heat flux from the urban canopy layer by the following equation:

$$Q_H = F_V \cdot Q_{HV} + F_U \cdot (Q_{HU} + \mathrm{Fix}_{AH}) \quad (4)$$

where Q_H is the total sensible heat flux. F_V and F_U are the fractional coverage of natural and urban surfaces, respectively. Q_{HV} is the sensible heat flux from Noah LSM for natural surfaces, and Q_{HU} is that from SLUCM for artificial surfaces. Fix_{AH} represents the fixed AH value for all urban areas (Chen et al., 2011). In ADDAH simulation case of this study, we basically follow the Eq. (4), but incorporate the gridded AH data estimated in Sect. 2.1 (Q_F) to replace the fixed AH value (Fix_{AH}) in order to considering the spatial distribution of AH fluxes. To account for temporal variability, the annual-mean AH fluxes in 2010 over the modeling area are further scaled with weighting functions dependent on local time of day (t_d) and time of year (m_y):

$$Q_F(t_d, m_y) = Q_F \cdot w_d(t_d) \cdot w_y(m_y) \quad (5)$$

ACPD
15, 32367–32412, 2015

where the diurnal cycles of w_d are obtained from the work of He et al. (2007) for the YRD region (shown in Fig. 3). And according to the findings of Sailor and Lu (2004) and Flanner (2009), the values of w_y for January and July are set to be 1.2 and 0.8, respectively.

2.4 Evaluation method and relevant observation data

Meteorological and chemical observation records are used to evaluate the model performance in this study. The mean bias (MB), root mean square error (RMSE) and correlation coefficient (CORR) between observation and the ADDAH model results are used to verify model performance. In statistics, they are usually defined as:

$$\mathrm{MB} = \frac{1}{N}\sum_{i=1}^{N}(S_i - O_i) \tag{6}$$

$$\mathrm{RMSE} = \sqrt{\frac{1}{N}\sum_{i}^{N}(S_i - O_i)^2} \tag{7}$$

$$\mathrm{CORR} = \frac{\sum_{1}^{N}(S_i - S_m)(O_i - O_m)}{\sqrt{\sum_{1}^{N}(S_i - S_m)^2}\sqrt{\sum_{1}^{N}(O_i - O_m)^2}} \tag{8}$$

where S_i is the simulation and O_i is the observation. S_m and O_m are average value of simulations and observations, respectively. In general, the model performance is acceptable if the values of MB and RMSE are close to zero and those of CORR are close to 1.

With respect to observed meteorological data, four observation sites are selected, which are NJ (32.00° N, 118.80° E) located in Nanjing, HF (31.87° N, 117.23° E) in

ACPD
15, 32367–32412, 2015

Hefei, HZ (30.23° N, 120.16° E) in Hangzhou, and SH (31.40° N, 121.46° E) in Shanghai, respectively (marked in Fig. 2b). Their time series of 2 m temperature, 10 m wind speed and 2 m relative humidity in January and July of 2010 can be obtained from hourly records of atmospheric sounding dataset compiled by University of Wyoming (http://weather.uwyo.edu). In order to evaluate model performance of chemical fields, hourly chemical series of PM_{10} and O_3 during the modeling period are acquired from Caochangmen (CCM) site. CCM is located in the central and highly residential area of Nanjing (32.06° N, 118.74° E), and is running by the Nanjing Environmental Monitoring Center. The assurance/quality control (QA/QC) procedures at CCM strictly follow the national standards.

3 Results and discussions

3.1 Spatial and temporal distribution of anthropogenic heat flux in the YRD region

Using the methodology outlined above in Sect. 2.1, we construct the spatial distribution of anthropogenic heat fluxes over the YRD region from 1990 to 2010 with a 5-year interval. Figure 4 illustrates the gridded distribution in 1995, 2000, 2005 and 2010 (The magnitude and spatial distribution pattern in 1990 are similar to 1995). Obviously, big cities, such as Shanghai, Nanjing, Hangzhou etc., have the largest values among neighboring areas from the early 1990s till now. Before 2000, except for some megacities, AH fluxes are generally less than 2.5 $W m^{-2}$ in most parts of the YRD region. However after 2000, the AH fluxes are more than 5 $W m^{-2}$ in many areas, with the high values over 25 $W m^{-2}$ centrally appearing along the Yangtze River, around Lake Taihu and beside Hangzhou Bay. The temporal variation of the spatial pattern fits in well with the economic boom in the YRD region over the past decades.

Being the largest city, Shanghai always has the highest anthropogenic heat emissions in the YRD region. As shown in Table 2, the annual mean value over the whole

ACPD
15, 32367–32412, 2015

administrative district is 5.47 $W m^{-2}$ in 1990 and 14.45 $W m^{-2}$ in 2010, with the annual growth of 0.45 $W m^{-2}$. While the annual mean values in the downtown area are much higher than the regional ones. And in recent years, the AH fluxes in the city center of Shanghai have exceeded 100 $W m^{-2}$, which is comparable to those in the most crowded megacities, such as Tokyo (Ichinose et al., 1999), Hong Kong (Flanner, 2009), London (Hamilton et al., 2009; Iamarino et al., 2012) and Singapore (Quah and Roth, 2012). In regard to Jiangsu Province and Zhejiang Province, the AH fluxes there also increase from 0.68 and 0.33 $W m^{-2}$ in 1990 to 2.61 and 1.63 $W m^{-2}$ in 2010. The regional annual mean values in Jiangsu higher than those in Zhejiang can be attributed to the facts that there are more large state-own enterprises (including petrochemical companies and power plants) in Jiangsu. Furthermore, the AH fluxes in the urban areas of Jiangsu and Zhejiang range from 20 to 50 $W m^{-2}$ in recent decade. These high values are close to those in Toulouse of France (Pigeon et al., 2007), Seoul of Korea (Lee et al., 2009), and some large US cities (Sailor and Lu, 2004; Fan and Sailor, 2005).

In 2010, nearly all areas of the YRD region have the AH fluxes more than 2.5 $W m^{-2}$ (shown in Fig. 4d). And high fluxes generally occur in and around the cities, such as Shanghai, Nanjing, Hangzhou, Yangzhou, Zhenjiang, Taizhou, Changzhou, Wuxi, Suzhou, Nantong, Huzhou, Jiaxing, Shaoxing, and Ningbo etc., with the typical values of 113.5, 50.2 and 39.3 $W m^{-2}$ in the urban areas of Shanghai, Jiangsu and Zhejiang, respectively (shown in Table 2). Comparing Fig. 4d with Fig. 1, we can easily find that the spatial distribution of AH based on the population reflects the economic activities in the YRD region as well, suggesting that our method is effective and the results are reasonable. Moreover, as shown in Table 2, parts of our conclusion can be supported by some other previous studies (He et al., 2007; Chen et al., 2012; Lu et al., 2014; Xie et al., 2015). Therefore, the gridded AH fluxes can be used in meso-scale meteorological and environmental modeling to investigate their impacts on urban climate and air quality.

ACPD
15, 32367–32412, 2015

3.2 Model evaluation for WRF/Chem

Table 3 shows the statistical comparisons between meteorological observations and the model results from both January and July simulations in ADDAH case. Mean values, MB, RMSE and CORR are all quantified for 2 m temperature (T_2), 2 m relative humidity (RH_2) and 10 m wind speed (WS_{10}) at four grids where NJ, HF, HZ and SH are located. As shown in Table 3, the correlation coefficients between observations and simulations (CORR) are over 0.9 in January and about 0.8 in July for T_2, more than 0.7 for RH_2 at most sites in both months, and close to 0.7 for WS_{10} in January. So WRF/Chem simulates the urban meteorological conditions over the YRD region quite well. With respect to T_2, the modeling results are slightly overvalued at all sites, which might be attributed to the uncertainty caused by urban canopy and surface parameters (Kusaka and Kimura, 2004; Chen et al., 2011; Liao et al., 2015). But the level of overestimation is acceptable, because the MB values of T_2 are only 1.1–1.7 °C in January and 0.7–2.0 °C in July with the RMSE of T_2 are 1.6–2.2 °C. The lowest value 0.7 °C for MB and the highest value 0.94 for CORR illustrate the best T_2 estimation at SH. For RH_2, compared with the observations, the simulation results are underestimated at all sites. Though worst simulation of RH_2 occurs at HF, the results are reasonable at other three sites. We find that the land-use dataset cannot well describe waters around HF. In view that HF is not in the center area of the YRD region, the deviation at HF cannot introduce crucial uncertainty into our main conclusion. In regard to WS_{10}, the modeling values from the ADDAH case are slightly overestimated at NJ, HF and HZ, whereas underestimated at SH. The MB for WS_{10} is generally less than 0.5 m s^{-1}, and the RMSE is less than 1.3 m s^{-1}. These over- or under-estimates are attributable to near-surface wind speed being influenced by local underlying surface characteristics more than other meteorological parameters. Further improvement of urban canopy parameters might improve the simulations (Zhang et al., 2010; Liao et al., 2015).

Figure 5 presents time series comparisons between the observation data of O_3 and PM_{10} at CCM and their modeling results from the ADDAH simulation case. Obviously,

ACPD
15, 32367–32412, 2015

WRF/Chem with gridded AH fluxes can capture diurnal variations and magnitude of these pollutants. For O_3, the correlation coefficient between observations and simulations (CORR) is 0.60 in January and 0.71 in July (statistically significant at 95 % confident level). And the value of MB is −0.8 ppb in January and 7.0 ppb in July, which can be explained that more solar radiation reaches to urban surface in July causing positive biases in T_2, and thereby produces more O_3 within PBL (Zhang et al., 2010; Liao et al., 2015). In regard to PM_{10}, the model prediction underestimates the concentration with MB being $-19.9\,\mu g\,m^{-3}$ in January and $-10.8\,\mu g\,m^{-3}$ in July respectively. This underestimate can be partially ascribed to positive biases of T_2, which induce an increase of PBL height and cause PM_{10} diluting within PBL (Liao et al., 2015). Furthermore, uncertainties in emissions may also cause these biases.

Liao et al. (2014) also simulated the same time periods in the YRD region by running WRF/Chem with a fixed AH flux in SLUCM. They found that the default SLUCM scheme tends to underestimate 2 m temperature in January but overestimate it in July, and overestimate the wind speed in both months. In a consequent, their chemical predictions are not so perfect as well, with the CORR of 0.44–0.52 for O_3 and 0.19–0.33 for PM_{10}. Compared with their results, our simulations accounting for the temporal and spatial distribution of AH improve the accuracy of the model results, and well predict the urban climate and air quality.

Generally, the WRF/Chem with gridded AH fluxes has relatively good capability on simulating urban climate and air quality over the YRD region in this study. Though the biases are still found, the difference between the modeling results from NONAH and ADDAH can still quantify the impacts of anthropogenic heat on meteorology and pollution, because all other conditions are the same in both simulations.

ACPD
15, 32367–32412, 2015

3.3 Impacts of AH on meteorological conditions

3.3.1 Horizontal meteorology changes

Figure 6 presents the monthly-averaged differences of main meteorological factors between ADDAH and NONAH (ADDAH-NONAH) over the modeling domain 3 (D03). Differences that are non-significant under the 95 % confidence level using student t test have been masked out. Obviously, the emissions of anthropogenic heat increase the sensible heat fluxes from the urban canopy layer over the YRD region. As shown in Fig. 6a and b, the spatial patterns of sensible heat changes in both January and July are similar to the spatial distribution of AH fluxes (Fig. 4d). High values of variation ($> 10\,W\,m^{-2}$) generally occur around mega-cities with a positive magnitude. For instance, in Shanghai, due to the maximum AH fluxes in the city center, the biggest increase of sensible heat flux for January can be $82\,W\,m^{-2}$, and the value is $75\,W\,m^{-2}$ in July. And in other cities, such as Hangzhou, Changzhou and Nantong etc., high values over $20\,W\,m^{-2}$ can be found in both months as well. In order to better understand the different behavior during the daytime and at night, the monthly-averaged diurnal variations of these modeled meteorological factors over the urban area of Shanghai in January and July are also calculated. As illustrated in Fig. 7, the adding AH fluxes lead to an increase of sensible heat flux (SHF) in both daytime and nighttime, with the daily mean increase of $22\,W\,m^{-2}$ for January and $20.5\,W\,m^{-2}$ for July. And the daytime increases are larger than those at night. On account that AH and its diurnal variation are only added to the sensible heat item, there are no significant differences between the ADDAH and the NONAH simulation for heat flux (GRDFLX) and latent heat flux (LH).

By adding more surface sensible heat into the atmosphere, the AH flux changes can influence the 2 m air temperature (T_2) as well. The patterns of the monthly-averaged T_2 changes (Fig. 6c and d) are similar to those of SHF (Fig. 6a and b). For city centers like Shanghai, Hangzhou and Nanjing, adding AH can lead to the increase of T_2 over 1 °C in January and over 0.5 °C in July, generating an enhanced Urban Heat Island.

ACPD
15, 32367–32412, 2015

And the maximum T_2 changes usually occur in the city center of Shanghai, with the typical value of 1.6 °C in January and 1.4 °C in July. These findings are comparable to the values estimated in megacities all over the world (Fan and Sailor, 2005; Ferguson and Woodbury, 2007; Chen et al., 2009; Zhu et al., 2010; Menberg et al., 2013; Wu and Yang, 2013; Bohnenstengel et al., 2014; Feng et al., 2014; Yu et al., 2014). Moreover, the mean increase of T_2 at night in January (1.2 °C) is larger than that in the daytime (1.0 °C), whereas the increase during the daytime and nighttime is all equal to 0.6 °C in July, suggesting that AH can help to form a weakened diurnal T_2 variation in winter.

The vertical air movement in PBL can be enhanced by the warming up of surface air temperature, which might increase the height of PBL (PBLH). Consequently, the adding AH fluxes make the PBLH rise up to over 50 m in January and more than 70 m in July over the YRD urban areas, with the maximum changes (140 m for January and 160 m for July) occurring in Shanghai (shown in Fig. 6e and f). And for both months, as shown in Fig. 7, the daytime relative increase of PBLH (10–15 %) is smaller than that at night (23–33 %), which can be attributed to the facts that the absolute PBLH values are lower and the air temperature increases more during the nighttime.

Figure 6g and h shows the changes in wind components over the YRD region, and demonstrate that AH can enhance the 10 m wind speed (WS_{10}) in the urban areas. The maximum increase is located in Shanghai, with the increment of 0.7 m s^{-1} (19 %) in January and 0.5 m s^{-1} (17 %) in July. In other cities like Hangzhou and Nanjing, the added value is only about 0.3 m s^{-1}. Over the YRD region, increase of WS_{10} is more obvious in January (Fig. 6g) than in July (Fig. 6h), and is slightly higher at night than in daytime (Fig. 7). As mentioned in previous studies, the above increase of wind speed can be ascribed to the strengthened urban-breeze circulation caused by the adding AH fluxes (Chen et al., 2009; Ryu et al., 2013; Yu et al., 2014), which can be further clarificated by the surface stronger convergence wind patterns occurring around the megacities shown in Fig. 6g and h. The simulated divergence at the surface near cities decreases 0.07–0.23 s^{-1} in January and 0.08–0.31 s^{-1} in July (not shown), also providing further evidence that the convergence is enhanced in these areas.

ACPD
15, 32367–32412, 2015

The strengthened urban-breeze circulation caused by adding AH can also enhance the vertical movement of atmosphere. As shown in Fig. 8a, the simulated vertical velocity above the megacities on 850 hPa layer increases about 2 cm s^{-1} in July, suggesting that the convection movements that can transport moisture and pollutants from surface to upper layer are strengthened in the urban areas. Thus, the spatial and vertical distributions of moisture are re-established. Figure 8c and d illustrates the spatial plots for monthly-averaged differences of 2 m relative humidity (RH_2) caused by adding AH (ADDAH-NONAH). The negative centers over the cities (the AH centers) can be seen in both January (−2 to −8 %) and July (−2 to −6 %), meaning the air near the surface became dryer. More moisture transported into the mid-troposphere (the vertical profile is discussed in Fig. 9g and h in details) might enhance rainfall inside urban areas as well. As shown in Fig. 8b, the increase of rainfall in July can be 72.4, 84.6 and 63.2 mm in Shanghai, Hangzhou and Ningbo, respectively. However, because of the negligible accumulative precipitation in winter, the increment of rainfall over the YRD region in January is ignorable (not shown).

3.3.2 Vertical meteorology changes

To better understand how AH change the vertical and spatial distribution of meteorology in the YRD region, we present changes (ADDAH-NONAH) of air temperature (T), vertical wind velocity (w), divergence (DIV) and water vapor mixing ratio (QVAPOR) along a cross-section from (28.9° N, 118.1° E) to (31.8° N, 122.6° E) as shown by the solid line AB in Fig. 2b. The vertical cross sections for T changes (Fig. 9a and b) illustrate that adding AH leads to an significant increase in air temperature near the surface around the cities (Shanghai and Hangzhou), while the changes are close to 0 in the rural areas and free troposphere. The monthly mean increment of T over Shanghai and Hangzhou at ground level in January (0.7 °C) is bigger than that in July (0.4 °C), which can be attributed to the facts that the relative increase of heat is higher in January due to background heat fluxes are much lower in winter.

ACPD
15, 32367–32412, 2015

The warming of air temperature near surface in cities, as well as the rising of PBLH in these areas (Fig. 6e and f), can generate an enhanced urban heat island. As shown in Fig. 9c and d, the vertical wind velocities above Shanghai and Hangzhou increase with added values of 0.3–0.7 $cm\,s^{-1}$ in both months, whereas w in the rural areas decreases about $-0.3\,m\,s^{-1}$ in January and $-0.5\,cm\,s^{-1}$ in July, suggesting that there are an enhanced upward movement in cities and an enhanced downward movement in countryside. We also analyze the divergence changes along the cross-section including Shanghai and Hangzhou (Fig. 9e and f). It can be seen that adding AH decreases DIV from surface to 750 m and increases DIV at higher levels, which means that there is a stronger convergence wind pattern in lower PBL and a more divergent wind pattern in higher PBL. This changing implies that the atmosphere is more unstable, and intends to promote the development of deep convection in troposphere. Consequently, impacted by the strengthened urban-breeze circulation, more moisture is transported from surface to the upper levels (over 1 km), with 0.6 $g\,kg^{-1}$ decrease of QVAPOR at the ground level and 0.1 $g\,kg^{-1}$ increase for the upper PBL in July as presented in Fig. 9g and h. Furthermore, the abovementioned vertical changes of w, DIV and QVAPOR are only restricted to the air column over the AH emission centers (Shanghai and Hangzhou) in January, while the changes distribute widely (the adding AH fluxes can impact wider areas) in July. This seasonal difference can be ascribed to the facts that the atmosphere is more stagnant in winter and more convective in summer.

3.4 Impacts of AH on air pollutants

3.4.1 Horizontal changes of O_3 and PM_{10}

Adding AH changes spatial and vertical meteorology conditions, and thereby undoubtedly affects the venting of air pollution. Due to PM_{10} is the main pollutant in YRD region (Wang et al., 2012; Xie et al., 2014; Liao et al., 2015), it is chosen as an indicator to show the changes of primary air pollutant transport and dispersion in this study. Figure 10 illustrates the influence of AH on PM_{10} spatial distribution in typical months of

ACPD
15, 32367–32412, 2015

winter and summer (differences that are non-significant at 95 % confidence level using t test are masked out). Results show that PM_{10} is reduced at all times around the cities, especially in Shanghai, Nanjing and Hangzhou. And the maximum decrease usually appears in Shanghai, with the monthly mean reduction of 29.3 $\mu g\,m^{-3}$ (24.5 %) in January and 26.6 $\mu g\,m^{-3}$ (18.8 %) in July. Compared with the distribution of AH emissions (Fig. 4) and meteorology changes (Fig. 6), the reduction in surface PM_{10} should be mainly related with the increase in PBLH, the rising up of surface wind speed and the enhanced upward movement of air, because these modifications of meteorological conditions caused by adding AH over the urban areas can facilitate PM_{10} transport and dispersion within the urban boundary layer. Furthermore, on account that the precipitation around the cities increases by 15–30 %, the wet scavenging can contribute to the reductions of the surface PM_{10} concentrations as well.

Spatial distribution of O_3 concentration can also be influenced by the changes of meteorological conditions due to adding AH. It should be noted that the increase of wind speed might facilitate O_3 transport, and the rising up of PBLH can lead to O_3 dilution within planetary boundary layer. Thus, the surface O_3 concentrations are seemingly reduced. However, unlike PM_{10}, O_3 is a secondary air pollutant formed by a series of complex chemical reactions involving oxides of nitrogen ($NO_x = NO + NO_2$) and volatile organic compounds (VOCs), so only considering the factors affecting O_3 transport and dispersion is not sufficient. In fact, O_3 changes are different from those of PM_{10}. As illustrated in Fig. 11a and b, the increases of surface O_3 level can be seen in both January and July over the YRD region, with large increase centers occurring in megacities. In January (Fig. 11a), the maximum O_3 difference appears in Shanghai, with the monthly mean increment of 2.5 ppb (18 %). In July (Fig. 11b), the highest O_3 change occurs in Hangzhou, with the added value of 4 ppb (15 %). And in the surrounding areas of these high value centers, increase of O_3 causing by AH can be over 0.5 ppb in January and more than 1 ppb in July. This change pattern and the magnitude are consistent with the findings reported in Beijing (Yu et al., 2014) and Seoul (Ryu et al., 2013).

ACPD
15, 32367–32412, 2015

Chemical direct and indirect effects should play a more important role in O_3 changes than other physical influencing factors. On the one hand, the rising up of air temperature (Fig. 6c and d) can directly accelerate O_3 formation by increasing the chemical reaction rates, and thereby straightly increase the O_3 level at surface. On the other hand, O_3 changes are inextricably influenced by the changes of NO_x (indirect chemical effects). Similar to other primary air pollutant (such as PM_{10}), NO_x at ground level are reduced in both January and July due mainly to the increase in PBLH, surface wind speed and upward air movement caused by adding AH (Fig. 11c and d). It was reported that the O_3 formation over the cities in the YRD region is sensitive to VOC (Xie et al., 2014), which means that a decrease in surface NO_x might lead to a slight increase of O_3 during the daytime. And at night, when the process of NO_x titration ($O_3 + NO \rightarrow O_2 + NO_2$) supersedes the O_3 sensitivity to be the governing factor of O_3 chemistry, less NO_x can only consume less O_3 as well. Consequently, the decrease in NO_x at the ground can result in the increase in O_3. This indirect function might be clearly illustrated in vertical distribution of O_3 changes in Sect. 3.4.2.

3.4.2 Vertical changes of O_3 and PM_{10}

Figure 12 shows the vertical plots on the cross-sectional line AB (presented in Fig. 2b) for the changes of chemical species impacted by adding AH (ADDAH-NONAH). Differences that are non-significant at 95 % confidence level using *t* test have been masked out. For the primary air pollutants such as PM_{10} and NO_x, the AH fluxes can decrease their concentrations near surface. As shown in Fig. 12a and b, in the atmosphere below 300 m above Shanghai and Hangzhou, the concentrations of PM_{10} decrease 2.3–16.2 $\mu g\,m^{-3}$ in January and 2.1–15.8 $\mu g\,m^{-3}$ in July, respectively. And surface NO_x concentrations near Shanghai and Hangzhou can be reduced over 15 ppb in both month as well (Fig. 12c and d). Meanwhile, it can be also found that there are increases in PM_{10} and NO_x concentrations at the upper levels over the cities. For instance, the added values of PM_{10} and NO_x can be more than 3 $\mu g\,m^{-3}$ and 3 ppb at about 1 km

ACPD
15, 32367–32412, 2015

above surface in January, respectively. This vertical changing pattern for primary chemical species is quite similar to that for water vapor (Fig. 9g and h), indicating that this is a reflection of the change in vertical transport patterns in the region due to AH (Yu et al., 2014). It should be noted that the maximum vertical changes of air pollutants in Hangzhou usually occur at about 1 km above surface, whereas those in Shanghai generally appear at higher levels (> 1 km), implying that more surface air pollutants in Shanghai might be transported into higher levels due to higher AH emissions in this biggest city in the YRD region. Furthermore, Fig. 13 shows the vertical profiles of the changes for PM_{10}, NO_x and O_3 caused by adding AH over Shanghai. In winter, the large increases of PM_{10} and NO_x appear at 500 to 1500 m above surface. But the maximum increases usually occur at more than 1.5 km above surface in summer. This phenomenon can be attributed to the facts that the atmosphere is more convective in summer than in winter.

On the contrary to the primary air pollutants, O_3 changes show increases near surface and decreases at the upper levels over the urban areas. Figure 12e and f illustrates that the increases of O_3 concentrations are limited within 400 m above the surface over the cities, with the high values of 2.6 ppb in January and 4.2 ppb in July. As mention in Sect. 3.4.1, this may be the result of both the increase in O_3 production caused by higher surface temperature and the decrease in O_3 depletion resulting from less surface NO. With respect to O_3 concentrations from 400 m to 1.5 km above surface, they generally decrease with the reduction values of more than 1 ppb in both January and July. Comparing Fig. 12e and f with Fig. 12c and d, we believe that the increases of NO_x concentrations at these upper levels can lead to the depletion of O_3, because of the VOC-sensitive O_3 chemistry in the daytime and NO_x titration at night in this region.

4 Conclusions

Urbanization impacts the atmospheric environment in many ways. Increases in pollution emissions, changes in land-use and excess anthropogenic heat (AH) emissions

ACPD
15, 32367–32412, 2015

from human activities caused by urbanization all can affect the city environment. In this paper, we specially address the impacts of AH on meteorological conditions and air pollution over the cities in the YRD region. Firstly, based on the energy consumption and the gridded population data, we estimate the spatial distribution of AH fluxes over the YRD region by a top-down energy inventory method. Secondly, the gridded AH data over the YRD region with the seasonal and the diurnal variation are added to the sensible heat flux from the urban canopy layer in the modified air quality model system WRF/Chem. Finally, the WRF/Chem is applied to investigate the impacts of AH on climate and air quality over the YRD region. Two simulation cases are conducted. One incorporates the single layer urban canopy model (SLUCM) with the gridded AH fluxes, while the other ignores the contribution of AH.

The results show that the AH flux in YRD region has been increased continually since 1990, especially after 2000. During the period between 1990 and 2010, the annual mean values of AH fluxes over Shanghai, Jiangsu and Zhejiang have been increased from 5.47 to 14.45, 0.68 to 2.61, and 0.33 to 1.63 $W m^{-2}$, respectively. High AH fluxes generally occur in and around the cities. And the typical values of AH in 2010 over the urban areas of Shanghai, Jiangsu and Zhejiang can reach 113.5, 50.2 and 39.3 $W m^{-2}$, respectively.

The model results of WRF/Chem fit the observational meteorological conditions and air quality very well. Inclusion of the AH can enhance the urban heat island in the cities over the YRD region, by increasing 2 m air temperature by more than 1 °C in January and over 0.5 °C in July with higher increment at night. It also increases the PBL heights, with the maximum changes of 140 m for January and 160 m for July in Shanghai. The strengthened urban-breeze circulation resulted from adding AH can enhance the 10 m wind speed and the vertical air movement as well. Thus, more moisture is transported from surface to the upper levels, with 0.6 $g kg^{-1}$ decrease at the ground level and 0.1 $g kg^{-1}$ increase for the upper PBL in July, which might induce the accumulative precipitation to increase by 15–30 % in Shanghai, Nanjing and Hangzhou.

ACPD
15, 32367–32412, 2015

Influenced by the modifications of meteorological conditions, the spatial and vertical distribution of air pollutants is re-established. With respect to the primary air pollutants (PM_{10} and NO_x), their transport and dispersion in PBL can be facilitated by the increases of PBLH, surface wind speed and upward air movement, which causes the decreases of concentrations near surface and the increases at the upper levels. Usually, PM_{10} can be reduced by 2–16 $\mu g\,m^3$ within 300 m above the surface of the cities, and added over 3 $\mu g\,m^{-3}$ in upper PBL. However, surface O_3 concentrations increase in the urban areas, with maximum changes of 2.5 ppb in January and 4 ppb in July. Besides the rising up of air temperature directly accelerating the surface O_3 formation, the decrease in NO_x at the ground can also result in the increase of surface O_3 due to the VOC-sensitive O_3 chemistry in the daytime and NO_x titration at night in this region. Furthermore, O_3 concentrations at higher levels are reduced by about 1 ppb due mainly to the increase of NO, and the impacts of AH are not only limited to the urban centers but also extended regionally.

Influence of anthropogenic heat emission due to urbanization on urban climate and air quality is undoubtedly an important and complex scientific issue. Our results show that the meteorology and air pollution predictions in and around large urban areas are highly sensitive to the anthropogenic heat inputs. In a consequent, for further understanding of urban atmospheric environment issues, good information on land use, detailed urban structure of the cities and more studies of the anthropogenic heat release should be better considered.

Acknowledgements. This work was supported by the National Natural Science Foundation of China (41475122), Public Welfare Project for Environmental Protection (201409008), Key Laboratory of South China Sea Meteorological Disaster Prevention and Mitigation of Hainan Province (SCSF201401), and Jiangsu Collaborative Innovation Center for Climate Change. The authors would like to thank the anonymous reviewers for their constructive and precious comments on this manuscript.

ACPD
15, 32367–32412, 2015

References

Block, A., Keuler, K., and Schaller, E.: Impacts of anthropogenic heat on regional climate patterns, Geophys. Res. Lett., 31, L12211, doi:10.1029/2004gl019852, 2004.

Bohnenstengel, S. I., Hamilton, I., Davies, M., and Belcher, S. E.: Impact of anthropogenic heat emissions on London's temperatures, Q. J. Roy. Meteor. Soc., 140, 687–698, doi:10.1002/qj.2144, 2014.

Chen, B., Shi, G. Y., Wang, B., Zhao, J. Q., and Tan, S. C.: Estimation of the anthropogenic heat release distribution in China from 1992 to 2009, Acta Meteorol. Sin., 26, 507–515, doi:10.1007/s13351-012-0409-y, 2012.

Chen, F. and Dudhia, J.: Coupling an advanced land surface-hydrology model with the Penn State-NCAR MM5 modeling system. Part I: Model implementation and sensitivity, Mon. Weather. Rev., 129, 569–585, doi:10.1175/1520-0493(2001)129<0569:Caalsh>2.0.Co;2, 2001.

Chen, F., Kusaka, H., Bornstein, R., Ching, J., Grimmond, C. S. B., Grossman-Clarke, S., Loridan, T., Manning, K. W., Martilli, A., Miao, S. G., Sailor, D., Salamanca, F. P., Taha, H., Tewari, M., Wang, X. M., Wyszogrodzki, A. A., and Zhang, C. L.: The integrated WRF/urban modelling system: development, evaluation, and applications to urban environmental problems, Int. J. Climatol., 31, 273–288, doi:10.1002/joc.2158, 2011.

Chen, Y., Jiang, W. M., Zhang, N., He, X. F., and Zhou, R. W.: Numerical simulation of the anthropogenic heat effect on urban boundary layer structure, Theor. Appl. Climatol., 97, 123–134, doi:10.1007/s00704-008-0054-0, 2009.

Crutzen, P. J.: New directions: the growing urban heat and pollution "island" effect – impact on chemistry and climate, Atmos. Environ., 38, 3539–3540, doi:10.1016/j.atmosenv.2004.03.032, 2004.

Fan, H. L. and Sailor, D. J.: Modeling the impacts of anthropogenic heating on the urban climate of Philadelphia: a comparison of implementations in two PBL schemes, Atmos. Environ., 39, 73–84, doi:10.1016/j.atmosenv.2004.09.031, 2005.

Feng, J. M., Wang, J., and Yan, Z. W.: Impact of anthropogenic heat release on regional climate in three vast urban agglomerations in China, Adv. Atmos. Sci., 31, 363–373, doi:10.1007/s00376-013-3041-z, 2014.

Ferguson, G. and Woodbury, A. D.: Urban heat island in the subsurface, Geophys. Res. Lett., 34, L23713, doi:10.1029/2007gl032324, 2007.

ACPD
15, 32367–32412, 2015

Flanner, M. G.: Integrating anthropogenic heat flux with global climate models, Geophys. Res. Lett., 36, L02801, doi:10.1029/2008gl036465, 2009.
Grimmond, C. S. B.: The suburban energy-balance – methodological considerations and results for a midlatitude west-coast city under winter and spring conditions, Int. J. Climatol., 12, 481–497, doi:10.1002/joc.3370120506, 1992.
Guenther, A., Karl, T., Harley, P., Wiedinmyer, C., Palmer, P. I., and Geron, C.: Estimates of global terrestrial isoprene emissions using MEGAN (Model of Emissions of Gases and Aerosols from Nature), Atmos. Chem. Phys., 6, 3181–3210, doi:10.5194/acp-6-3181-2006, 2006.
Hamilton, I. G., Davies, M., Steadman, P., Stone, A., Ridley, I., and Evans, S.: The significance of the anthropogenic heat emissions of London's buildings: a comparison against captured shortwave solar radiation, Build. Environ., 44, 807–817, doi:10.1016/j.buildenv.2008.05.024, 2009.
He, X. F., Jiang, W. M., Chen, Y., and Liu, G.: Numerical simulation of the impacts of anthropogenic heat on the structure of the urban boundary layer, Chinese J. Geophys.-Ch., 50, 74–82, 2007.
Iamarino, M., Beevers, S., and Grimmond, C. S. B.: High-resolution (space, time) anthropogenic heat emissions: London 1970–2025, Int. J. Climatol., 32, 1754–1767, doi:10.1002/joc.2390, 2012.
Ichinose, T., Shimodozono, K., and Hanaki, K.: Impact of anthropogenic heat on urban climate in Tokyo, Atmos. Environ., 33, 3897–3909, doi:10.1016/S1352-2310(99)00132-6, 1999.
Janjic, Z. I.: The step-mountain eta coordinate model – further developments of the convection, viscous sublayer, and turbulence closure schemes, Mon. Weather. Rev., 122, 927–945, doi:10.1175/1520-0493(1994)122<0927:Tsmecm>2.0.Co;2, 1994.
Kain, J. S.: The Kain–Fritsch convective parameterization: an update, J. Appl. Meteorol., 43, 170–181, doi:10.1175/1520-0450(2004)043<0170:Tkcpau>2.0.Co;2, 2004.
Khan, S. M. and Simpson, R. W.: Effect of a heat island on the meteorology of a complex urban airshed, Bound-Lay. Meteorol., 100, 487–506, doi:10.1023/A:1019284332306, 2001.
Kikegawa, Y., Genchi, Y., Yoshikado, H., and Kondo, H.: Development of a numerical simulation system toward comprehensive assessments of urban warming countermeasures including their impacts upon the urban buildings' energy-demands, Appl. Energ., 76, 449–466, doi:10.1016/S0306-2619(03)00009-6, 2003.

ACPD
15, 32367–32412, 2015

Kim, H. J. and Wang, B.: Sensitivity of the WRF model simulation of the East Asian summer monsoon in 1993 to shortwave radiation schemes and ozone absorption, Asia-Pac. J. Atmos. Sci., 47, 167–180, doi:10.1007/s13143-011-0006-y, 2011.

Kusaka, H. and Kimura, F.: Coupling a single-layer urban canopy model with a simple atmospheric model: impact on urban heat island simulation for an idealized case, J. Meteorol. Soc. Jpn., 82, 67–80, doi:10.2151/Jmsj.82.67, 2004.

Lee, S. H., Song, C. K., Baik, J. J., and Park, S. U.: Estimation of anthropogenic heat emission in the Gyeong-In region of Korea, Theor. Appl. Climatol., 96, 291–303, doi:10.1007/s00704-008-0040-6, 2009.

Li, L., Chen, C. H., Fu, J. S., Huang, C., Streets, D. G., Huang, H. Y., Zhang, G. F., Wang, Y. J., Jang, C. J., Wang, H. L., Chen, Y. R., and Fu, J. M.: Air quality and emissions in the Yangtze River Delta, China, Atmos. Chem. Phys., 11, 1621–1639, doi:10.5194/acp-11-1621-2011, 2011.

Liao, J. B., Wang, T. J., Wang, X. M., Xie, M., Jiang, Z. Q., Huang, X. X., and Zhu, J. L.: Impacts of different urban canopy schemes in WRF/Chem on regional climate and air quality in Yangtze River Delta, China, Atmos. Res., 145, 226–243, doi:10.1016/j.atmosres.2014.04.005, 2014.

Liao, J. B., Wang, T. J., Jiang, Z. Q., Zhuang, B. L., Xie, M., Yin, C. Q., Wang, X. M., Zhu, J. L., Fu, Y., and Zhang, Y.: WRF/Chem modeling of the impacts of urban expansion on regional climate and air pollutants in Yangtze River Delta, China, Atmos. Environ., 106, 204–214, doi:10.1016/j.atmosenv.2015.01.059, 2015.

Lin, Y. L., Farley, R. D., and Orville, H. D.: Bulk parameterization of the snow field in a cloud model, J. Clim. Appl. Meteorol., 22, 1065–1092, doi:10.1175/1520-0450(1983)022<1065:Bpotsf>2.0.Co;2, 1983.

Liu, Q., Lam, K. S., Jiang, F., Wang, T. J., Xie, M., Zhuang, B. L., and Jiang, X. Y.: A numerical study of the impact of climate and emission changes on surface ozone over south China in autumn time in 2000–2050, Atmos. Environ., 76, 227–237, doi:10.1016/j.atmosenv.2013.01.030, 2013.

Lu, Y., Wang, Q. G., Zhai, Y. R., Song, Y. Y., Zhang, Y. Y., and Sun, P.: Anthropogenic heat emissions in the Yangtze River Delta region, China Environmental Science, 34, 295–301, 2014.

ACPD
15, 32367–32412, 2015

Menberg, K., Bayer, P., Zosseder, K., Rumohr, S., and Blum, P.: Subsurface urban heat islands in German cities, Sci. Total. Environ., 442, 123–133, doi:10.1016/j.scitotenv.2012.10.043, 2013.

Mlawer, E. J., Taubman, S. J., Brown, P. D., Iacono, M. J., and Clough, S. A.: Radiative transfer for inhomogeneous atmospheres: RRTM, a validated correlated-k model for the longwave, J. Geophys. Res.-Atmos., 102, 16663–16682, doi:10.1029/97jd00237, 1997.

Offerle, B., Grimmond, C. S. B., and Fortuniak, K.: Heat storage and anthropogenic heat flux in relation to the energy balance of a central European city centre, Int. J. Climatol., 25, 1405–1419, doi:10.1002/joc.1198, 2005.

Oke, T. R.: The urban energy-balance, Prog. Phys. Geog., 12, 471–508, doi:10.1177/030913338801200401, 1988.

Pigeon, G., Legain, D., Durand, P., and Masson, V.: Anthropogenic heat release in an old European agglomeration (Toulouse, France), Int. J. Climatol., 27, 1969–1981, doi:10.1002/joc.1530, 2007.

Sailor, D. J.: A review of methods for estimating anthropogenic heat and moisture emissions in the urban environment, Int. J. Climatol., 31, 189–199, doi:10.1002/joc.2106, 2011.

Sailor, D. J. and Lu, L.: A top-down methodology for developing diurnal and seasonal anthropogenic heating profiles for urban areas, Atmos. Environ., 38, 2737–2748, doi:10.1016/j.atmosenv.2004.01.034, 2004.

Streets, D. G., Yarber, K. F., Woo, J. H., and Carmichael, G. R.: Biomass burning in Asia: annual and seasonal estimates and atmospheric emissions, Global Biogeochem. Cy., 17, 1099, doi:10.1029/2003gb002040, 2003.

Wang, T. J., Jiang, F., Deng, J. J., Shen, Y., Fu, Q. Y., Wang, Q., Fu, Y., Xu, J. H., and Zhang, D. N.: Urban air quality and regional haze weather forecast for Yangtze River Delta region, Atmos. Environ., 58, 70–83, doi:10.1016/j.atmosenv.2012.01.014, 2012.

Wang, X. M., Chen, F., Wu, Z. Y., Zhang, M. G., Tewari, M., Guenther, A., and Wiedinmyer, C.: Impacts of weather conditions modified by urban expansion on surface ozone: comparison between the Pearl River Delta and Yangtze River Delta regions, Adv. Atmos. Sci., 26, 962–972, doi:10.1007/s00376-009-8001-2, 2009.

Wang, X. M., Sun, X. G., Tang, J. P., and Yang, X. Q.: Urbanization-induced regional warming in Yangtze River Delta: potential role of anthropogenic heat release, Int. J. Climatol., in press, doi:10.1002/joc.4296, 2015.

ACPD
15, 32367–32412, 2015

Wu, K. and Yang, X. Q.: Urbanization and heterogeneous surface warming in eastern China, Chinese Sci. Bull., 58, 1363–1373, doi:10.1007/s11434-012-5627-8, 2013.

Xie, M., Zhu, K. G., Wang, T. J., Yang, H. M., Zhuang, B. L., Li, S., Li, M. G., Zhu, X. S., and Ouyang, Y.: Application of photochemical indicators to evaluate ozone nonlinear chemistry and pollution control countermeasure in China, Atmos. Environ., 99, 466–473, doi:10.1016/j.atmosenv.2014.10.013, 2014.

Xie, M., Zhu, K. G., Wang, T. J., Feng, W., Zhu, X. S., Chen, F., Ouyang, Y., and Liu, Z. J.: Study on the distribution of anthropogenic heat flux over China, China Environmental Science, 35, 728–734, 2015.

Yang, W. M., Jiang, H., Yu, X. Y., and Cui, X. F.: Review of research on anthropogenic heat under climate change, Prog. Geogr., 33, 1029–1038, 2014.

Zaveri, R. A. and Peters, L. K.: A new lumped structure photochemical mechanism for large-scale applications, J. Geophys. Res.-Atmos., 104, 30387–30415, doi:10.1029/1999jd900876, 1999.

Zaveri, R. A., Easter, R. C., Fast, J. D., and Peters, L. K.: Model for Simulating Aerosol Interactions and Chemistry (MOSAIC), J. Geophys. Res.-Atmos., 113, D13204, doi:10.1029/2007jd008782, 2008.

Zhang, N., Gao, Z. Q., Wang, X. M., and Chen, Y.: Modeling the impact of urbanization on the local and regional climate in Yangtze River Delta, China, Theor. Appl. Climatol., 102, 331–342, doi:10.1007/s00704-010-0263-1, 2010.

Zhang, Q., Streets, D. G., Carmichael, G. R., He, K. B., Huo, H., Kannari, A., Klimont, Z., Park, I. S., Reddy, S., Fu, J. S., Chen, D., Duan, L., Lei, Y., Wang, L. T., and Yao, Z. L.: Asian emissions in 2006 for the NASA INTEX-B mission, Atmos. Chem. Phys., 9, 5131–5153, doi:10.5194/acp-9-5131-2009, 2009.

Zhu, K., Blum, P., Ferguson, G., Balke, K. D., and Bayer, P.: The geothermal potential of urban heat islands, Environ. Res. Lett., 5, 044002, doi:10.1088/1748-9326/5/4/044002, 2010.

ACPD
15, 32367–32412, 2015

Table 1. The grid settings, physics and chemistry options used in this study for WRF/Chem.

Items	Contents
Dimensions (x, y)	(85,75), (76,70), (76,70)
Grid size (km)	81, 27, 9
Time step (s)	360
Microphysics	Purdue Lin microphysics scheme (Lin et al., 1983)
Long-wave radiation	RRTM scheme (Mlawer et al., 1997)
Short-wave radiation	Goddard scheme (Kim and Wang, 2011)
Cumulus parameterization	Kain–Fritsch scheme, only for D01 and D02 (Kain, 2004)
Land surface	Noah land surface model (Chen and Dudhia, 2001)
Planetary boundary layer	Mellor–Yamada–Janjic scheme (Janjic, 1994)
Urban canopy model	SLUCM (Kusaka and Kimura, 2004)
Gas-phase chemistry	CBM-Z (Zaveri and Peters, 1999)
Aerosol module	MOSAIC using 8 sectional aerosol bins (Zaveri et al., 2008)

ACPD
15, 32367–32412, 2015

Table 2. The statistics of annual average anthropogenic heat flux in different administrative district over the YRD region ($W m^{-2}$).

Province or Municipality		This study 1990	1995	2000	2005	2010	Previous results (year)	References
Shanghai	Regional	5.47	7.85	9.2	12.39	14.45	16.54 (2008) 16.10 (2010)	Chen et al. (2012) Lu et al. (2014)
	Downtown	42	60.8	71.6	96.9	113.5	117.7 (2010)	Lu et al. (2014)
Jiangsu	Regional	0.68	0.94	0.99	1.83	2.61	2.32 (2008)	Chen et al. (2012)
	Downtown	5.1	9.5	12.5	28.6	50.2	40 (Nanjing, 2007) 20–70 (2010)	He et al. (2007) Lu et al. (2014)
Zhejiang	Regional	0.33	0.54	0.73	1.25	1.63	1.60 (2008)	Chen et al. (2012)
	Downtown	2.7	7.4	12.1	25.1	39.3	50 (Hangzhou, 2007) 20–70 (2010)	He et al. (2007) Lu et al. (2014)

Regional represents the average value over the whole area of an administrative district, while Downtown represents the high value in the city center.

ACPD
15, 32367–32412, 2015

Table 3. The statistics of meteorological conditions from the ADDAH simulation at four sites.

Vars[a]	Sites[b]	January Mean[c] OBS[e]	SIM[f]	MB	RMSE	CORR[d]	July Mean[c] OBS[e]	SIM[f]	MB	RMSE	CORR[d]
T_2 (°C)	NJ	3.5	5.1	1.6	2.2	0.92	28.2	30.2	2.0	2.0	0.83
	HZ	5.7	7.4	1.7	1.9	0.93	28.7	30.5	1.8	2.2	0.80
	HF	3.6	5.1	1.5	2.2	0.91	28.9	30.6	1.7	2.1	0.76
	SH	5.6	6.7	1.1	1.6	0.94	28.8	29.5	0.7	1.7	0.85
RH_2 (%)	NJ	65	53	−12	14	0.74	76	68	−9	10	0.71
	HZ	67	60	−7	10	0.83	74	70	−4	17	0.71
	HF	71	51	−20	13	0.75	88	69	−19	12	0.62
	SH	70	64	−6	11	0.79	76	72	−4	11	0.77
WS_{10} ($m s^{-1}$)	NJ	2.6	3.1	0.5	1.2	0.61	2.9	3.2	0.3	1.3	0.53
	HZ	2.5	2.6	0.1	1.0	0.69	2.4	2.5	0.1	1.3	0.34
	HF	2.6	2.9	0.3	1.1	0.67	2.3	2.7	0.4	1.2	0.40
	SH	4.1	3.8	−0.3	1.2	0.78	4.1	3.6	−0.5	1.2	0.66

[a] Vars represents variables, including temperature at 2 m (T_2), relative humidity at 2 m (RH_2) and wind speed at 10 m (WS_{10}).
[b] Sites indicates the observation meteorological sites used in this study, including NJ in Nanjing, HF in Hefei, HZ in Hangzhou and SH in Shanghai.
[c] Mean indicates the average value.
[d] Statistically significant at 95 % confident level.
[e] OBS presents observation data.
[f] SIM represents simulation results from WRF/Chem

ACPD
15, 32367–32412, 2015

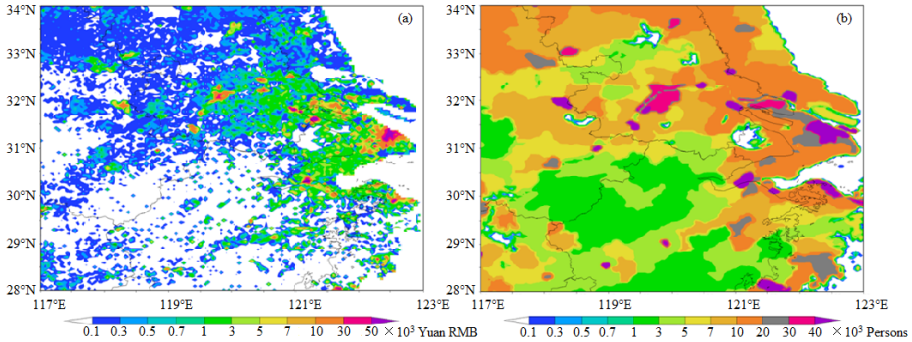

Figure 1. Spatial distribution of Gross Domestic Product **(a)** and population **(b)** in 2010 over the region between (117° E, 28° N) and (123° E, 34° N) with the resolution of 2.5 arcmin. Data are obtained from the website http://sedac.ciesin.columbia.edu/gpw.

ACPD
15, 32367–32412, 2015

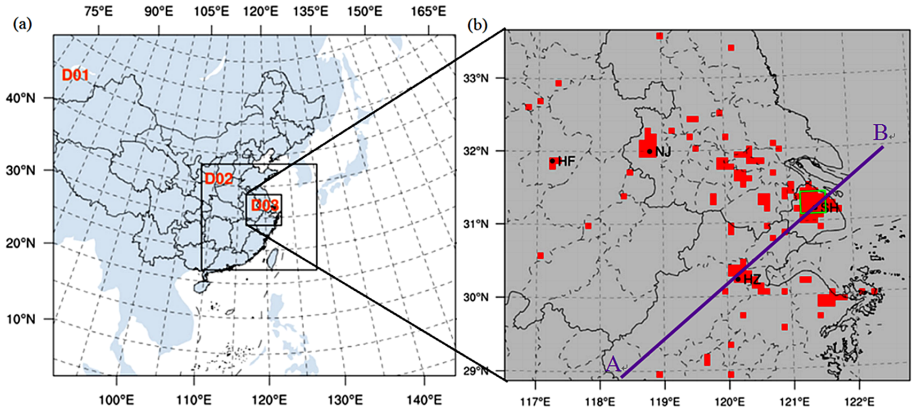

Figure 2. The three nested modeling domains **(a)** and MODIS urban land-use category dataset used in D03, with the locations of the four meteorology observation sites **(b)**. SH, HZ, NJ and HF in **(b)** represent Shanghai, Hangzhou, Nanjing and Hefei, respectively. Line AB denotes the location of the vertical cross section used in Figs. 9 and 12.

ACPD
15, 32367–32412, 2015

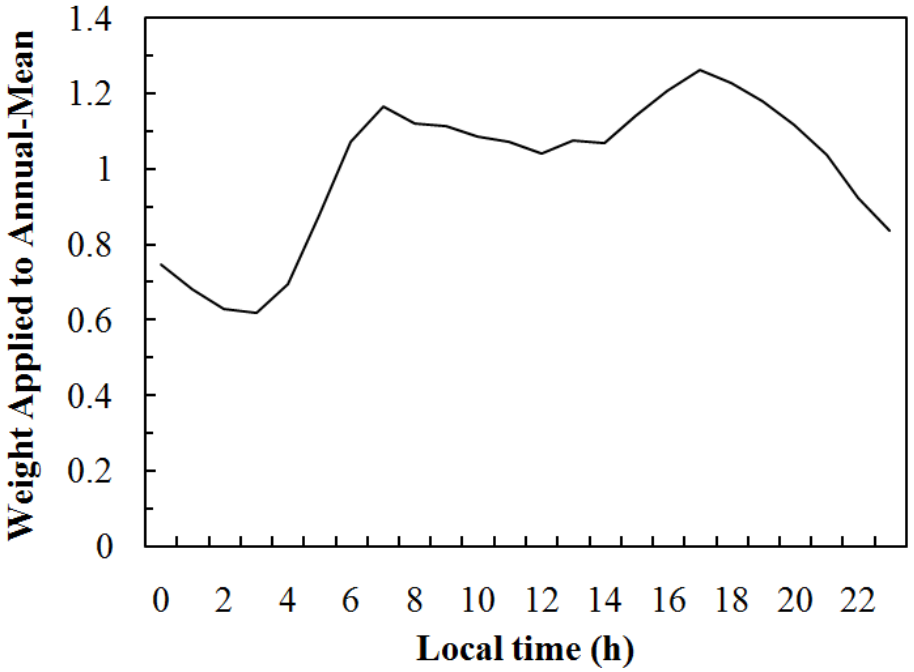

Figure 3. Diurnal variation of anthropogenic heat flux based on He et al. (2007), applied as weights to the annual-mean flux.

ACPD
15, 32367–32412, 2015

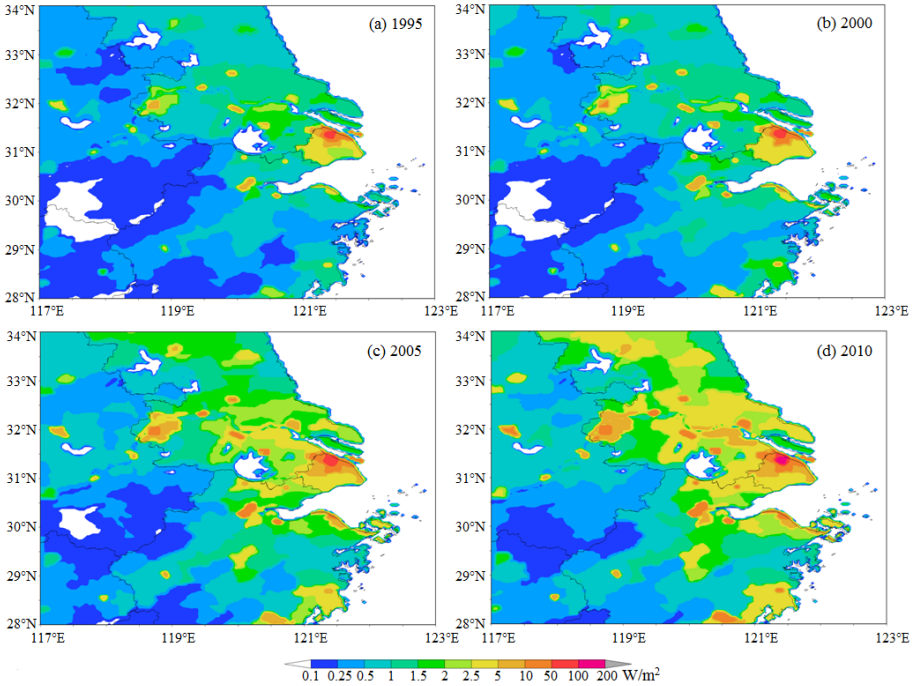

Figure 4. Estimates of annual-mean anthropogenic heat fluxes resulting from the consumption of non-renewable energy sources (coal, petroleum, natural gas, and electricity) and human metabolism between (117° E, 28° N) and (123° E, 34° N) with the resolution of 2.5 arcmin for 1995 **(a)**, 2000 **(b)**, 2005 **(c)** and 2010 **(d)**, respectively.

ACPD
15, 32367–32412, 2015

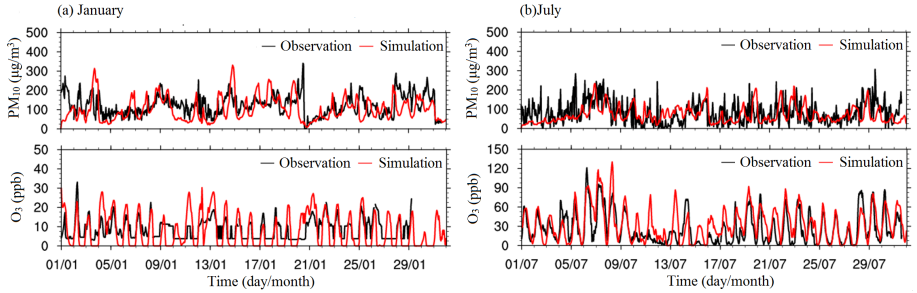

Figure 5. Hourly variations of PM_{10} ($\mu g\,m^{-3}$) and O_3 (ppb) from the observation data and the ADDAH simulation results at CCM monitoring site in Nanjing for January **(a)** and July **(b)**.

ACPD
15, 32367–32412, 2015

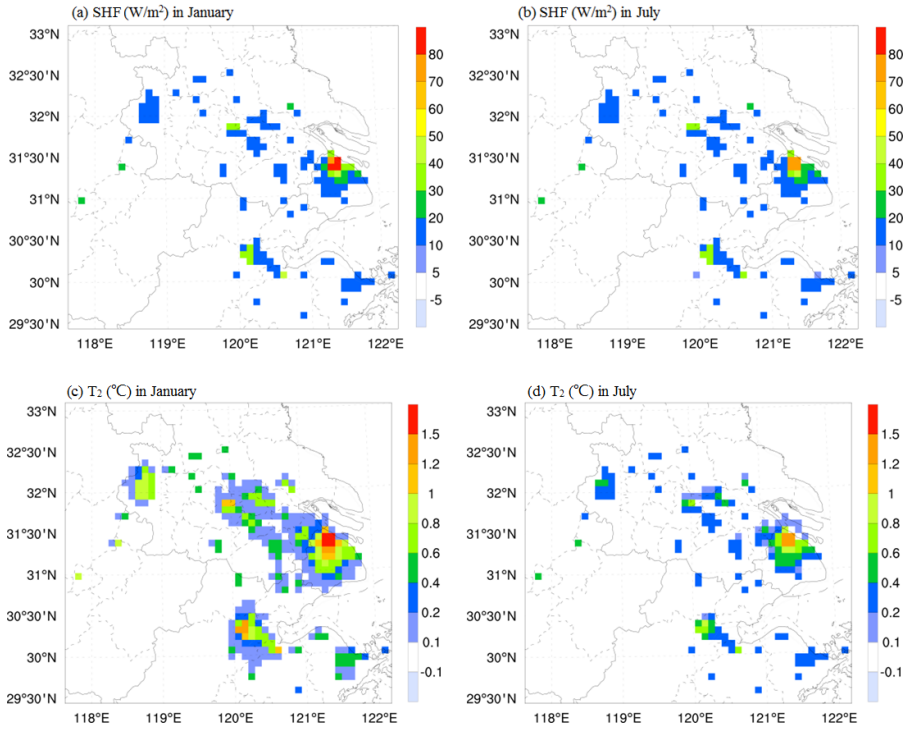

Figure 6.

ACPD
15, 32367–32412, 2015

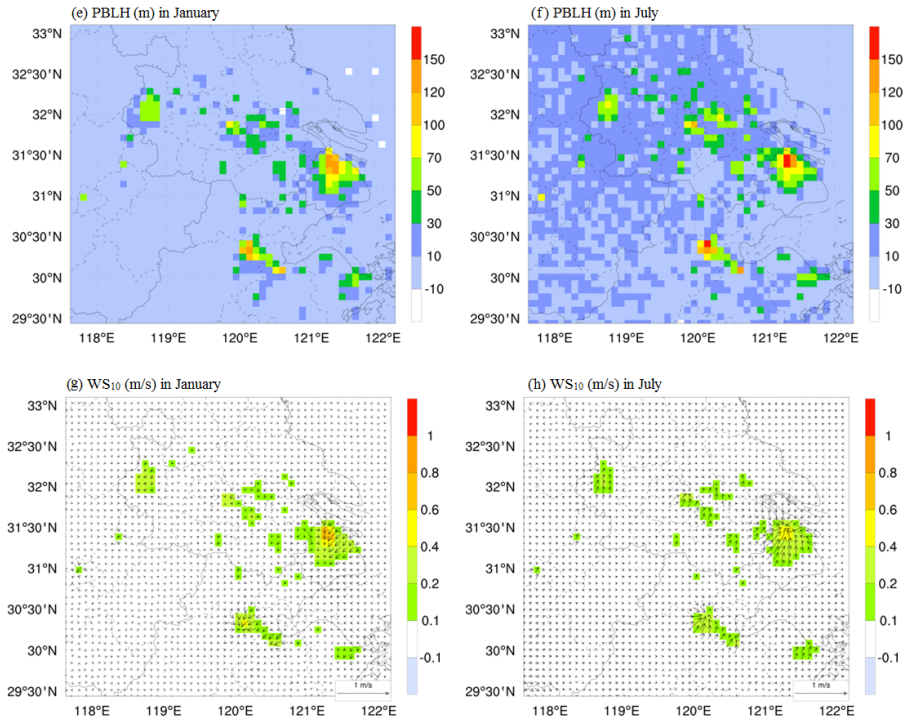

Figure 6. The spatial distributions of monthly-averaged differences for sensible heat flux (SHF), air temperature at 2 m (T_2), the height of planetary boundary layer (PBLH), and wind speed (WS_{10}) at 10 m between ADDAH and NONAH (ADDAH-NONAH). **(a, c, e, g)** show changes in January. **(b, d, f, h)** illustrate variations in July. The arrows in **(g)** and **(h)** are the differences of wind fields. Differences that are non-significant under the 95 % confidence level (student *t* test) are masked out.

ACPD
15, 32367–32412, 2015

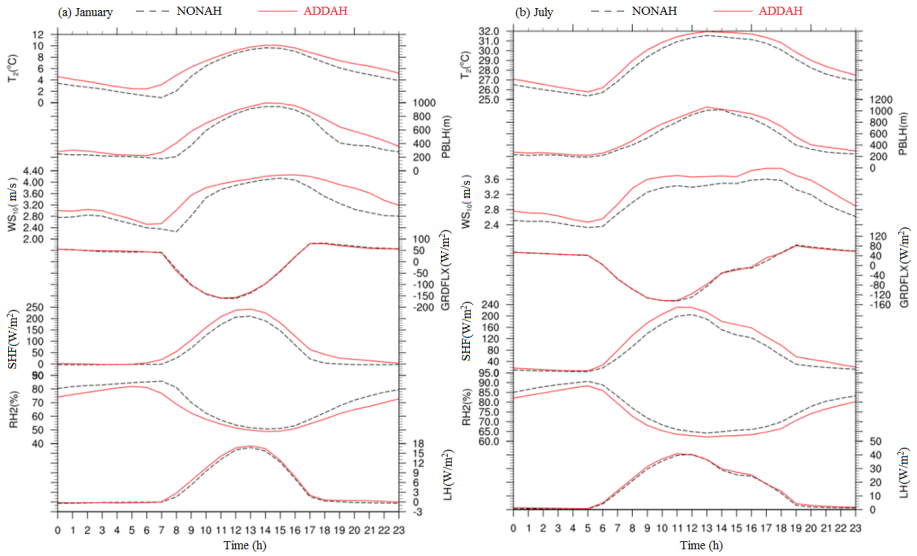

Figure 7. The monthly-averaged diurnal variations of modeled meteorological factors in January **(a)** and July **(b)** over the urban area of Shanghai. NONAH and ADDAH represent the simulation cases with and without AH fluxes, respectively. LH means latent heat. SHF indicates sensible heat flux. GRDFLX represents heat flux from ground level. T_2, RH_2, WS_{10}, and PBLH indicate 2 m air temperature (°C), 2 m relative humidity (%), 10 m wind speed ($m\,s^{-1}$) and the height of planetary boundary layer (m), respectively.

ACPD
15, 32367–32412, 2015

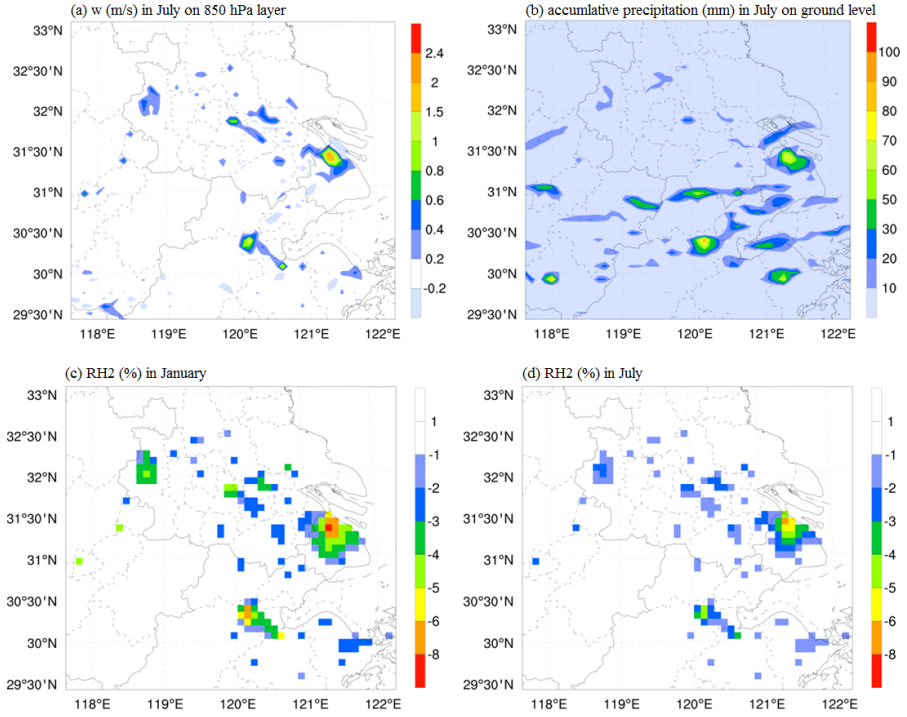

Figure 8. The spatial distributions of monthly-averaged differences for 2 m relative humidity (RH_2), surface accumulative precipitation and vertical wind velocity on 850 hPa layer (w) between ADDAH and NONAH (ADDAH-NONAH). Differences that are non-significant under the 95 % confidence level (student t test) are masked out.

ACPD
15, 32367–32412, 2015

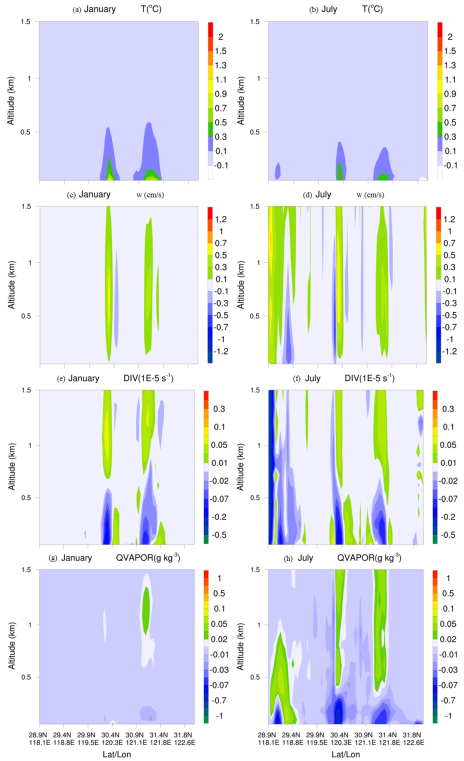

Figure 9. The vertical distribution of monthly-averaged differences for air temperature (T), vertical wind velocity (w), divergence (DIV), and water vapor mixing ratio (QVAPOR) between ADDAH and NONAH (ADDAH-NONAH) from surface to 1.5 km altitude along the line AB (shown in Fig. 2b). **(a, c, e, g)** show changes in January. **(b, d, f, h)** illustrate variations in July. Differences that are non-significant under the 95 % confidence level (student t test) are masked out.

ACPD
15, 32367–32412, 2015

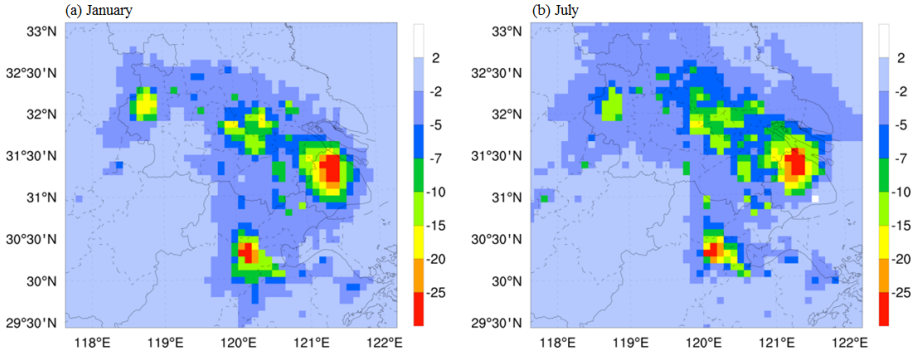

Figure 10. The spatial distributions of monthly-averaged differences for PM_{10} between ADDAH and NONAH (ADDAH-NONAH). Differences that are non-significant under the 95 % confidence level (student *t* test) are masked out.

ACPD
15, 32367–32412, 2015

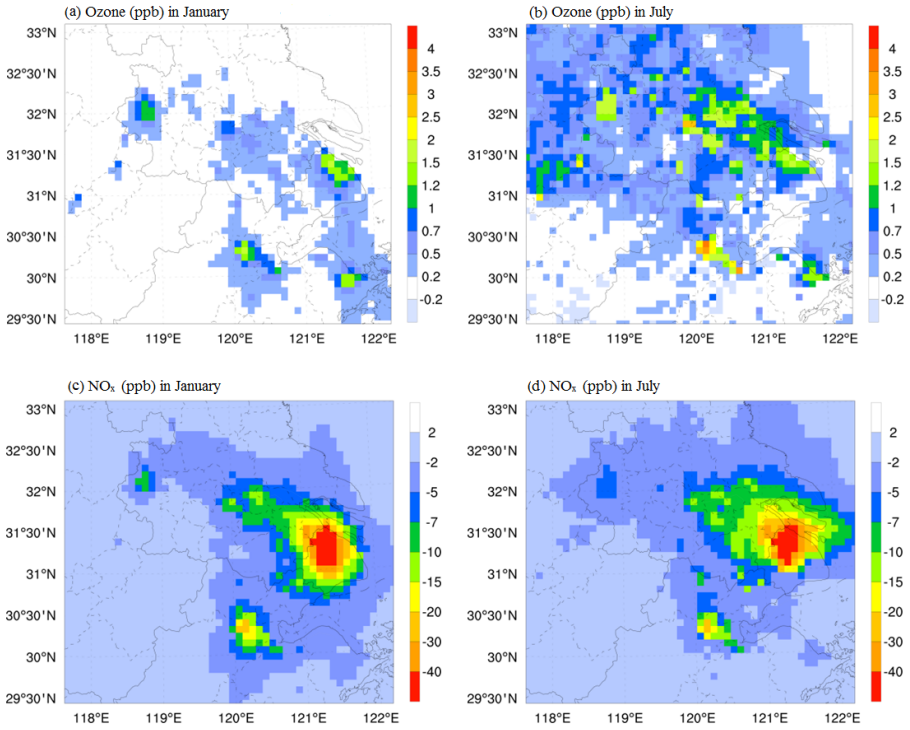

Figure 11. The spatial distributions of monthly-averaged differences for O_3 and its precursor NO_x between ADDAH and NONAH (ADDAH-NONAH). Differences that are non-significant under the 95 % confidence level (student *t* test) are masked out.

ACPD
15, 32367–32412, 2015

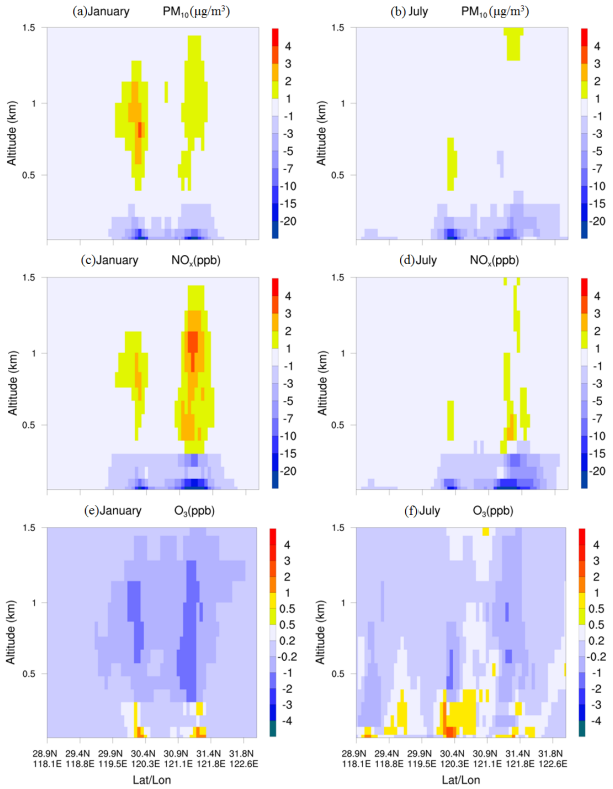

Figure 12. The vertical distribution of monthly-averaged differences for PM_{10}, NO_x and O_3 between ADDAH and NONAH (ADDAH-NONAH) from surface to 1.5 km altitude along the line AB (shown in Fig. 2b). **(a, c, e)** show changes in January. **(b, d, f)** illustrate variations in July. Differences that are non-significant under the 95 % confidence level (student *t* test) are masked out.

ACPD
15, 32367–32412, 2015

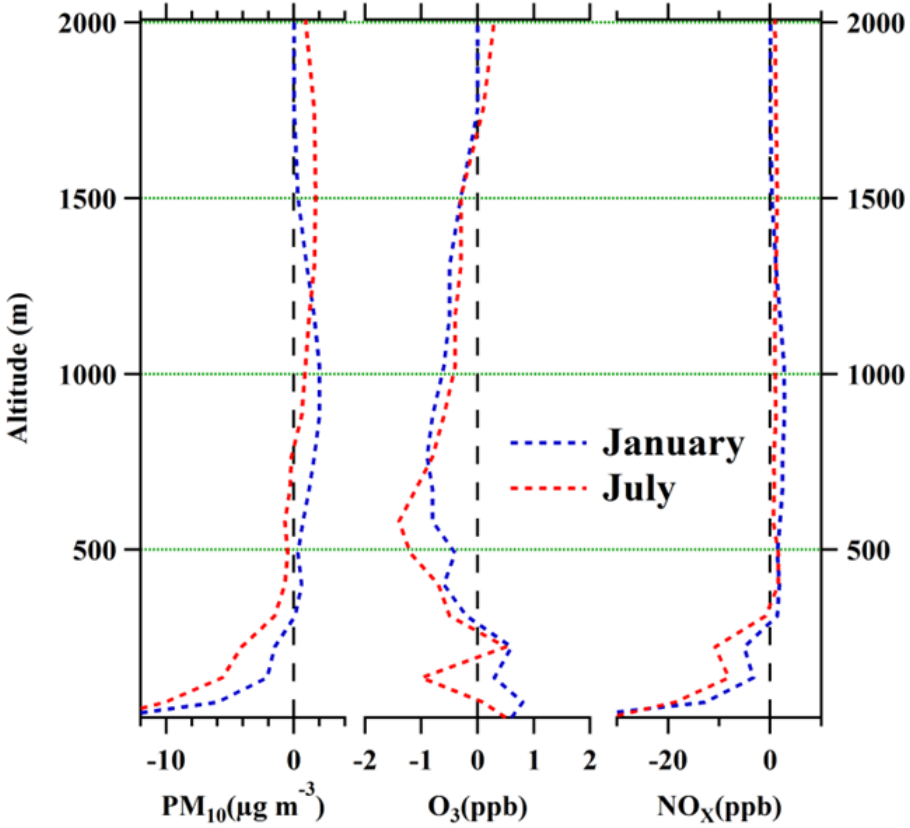

Figure 13. The vertical profiles of monthly-averaged differences for PM_{10}, NO_x and O_3 between ADDAH and NONAH (ADDAH-NONAH) over Shanghai.

ACPD
15, 32367–32412, 2015